Research Square

Preprints are preliminary reports that have not undergone peer review.
They should not be considered conclusive, used to inform clinical practice,
or referenced by the media as validated information.

Lindera aggregata -derived Extracellular Vesicles Target Inflammation for Alleviating IBD associated psychiatric disorders via Microbiota-Gut-Brain Axis

Xiaoting Zhang
College of Pharmaceutical Sciences, Zhejiang University of Technology, Hangzhou, Zhejiang 310014, China

Jigeng Cao
College of Pharmaceutical Sciences, Zhejiang University of Technology, Hangzhou, Zhejiang 310014, China

Tingting Hu
Department of Transfusion，Minhang Hospital, Fudan University

Chengwen He
Department of Transfusion medicine, Zhejiang Provincial People's Hospital (Affiliated People's Hospital), Hangzhou Medical College, Hangzhou, Zhejiang 310014, China

Wei Xu
Department of Transfusion medicine, Zhejiang Provincial People's Hospital (Affiliated People's Hospital), Hangzhou Medical College, Hangzhou, Zhejiang 310014, China

Kai Yu
School of Medical Technology and Information Engineering, Zhejiang Chinese Medical University, Hangzhou, Zhejiang, 310053, China

Ke Hao
Department of Transfusion medicine, Zhejiang Provincial People's Hospital (Affiliated People's Hospital), Hangzhou Medical College, Hangzhou, Zhejiang 310014, China

Aibo Xu
Department of Transfusion medicine, Zhejiang Provincial People's Hospital (Affiliated People's Hospital), Hangzhou Medical College, Hangzhou, Zhejiang 310014, China

Kaixuan Li
Department of Transfusion medicine, Zhejiang Provincial People's Hospital (Affiliated People's Hospital), Hangzhou Medical College, Hangzhou, Zhejiang 310014, China

Qian Tong
Department of Transfusion medicine, Zhejiang Provincial People's Hospital (Affiliated People's Hospital), Hangzhou Medical College, Hangzhou, Zhejiang 310014, China

Zhen Wang

Department of Transfusion medicine, Zhejiang Provincial People's Hospital (Affiliated People's Hospital), Hangzhou Medical College, Hangzhou, Zhejiang 310014, China

Youmin Ying

College of Pharmaceutical Sciences, Zhejiang University of Technology, Hangzhou, Zhejiang 310014, China

Kaiqiang Li

likaiqiang@hmc.edu.cn

Department of Transfusion medicine, Zhejiang Provincial People's Hospital (Affiliated People's Hospital), Hangzhou Medical College, Hangzhou, Zhejiang 310014, China

---

Research Article

Keywords: Inflammatory bowel disease, anxiety, depression and cognitive impairment, Plant-derived Extracellular Vesicles, microbiota-gut-brain axis

Posted Date: November 13th, 2026

DOI: https://doi.org/10.21203/rs.3.rs-11305681/v1

License: This work is licensed under a Creative Commons Attribution 4.0 International License. Read Full License

Additional Declarations: No competing interests reported.

Lindera aggregata -derived Extracellular Vesicles Target Inflammation for Alleviating IBD associated psychiatric disorders via Microbiota-Gut-Brain Axis

Xiaoting Zhang [a,1], Jigeng Cao [a,1], Tingting Hu [b,1], Chengwen He [c,d,1], Wei Xu [c], Kai Yu [e], Ke Hao [c,d], Aibo Xu [c,d], Kaixuan Li [c,d], Qian Tong [c,d], Zhen Wang [c,d,*], Youmin Ying [a,*], Kaiqiang Li [c,d*]

[a] College of Pharmaceutical Sciences, Zhejiang University of Technology, Hangzhou, Zhejiang 310014, China

[b] Department of Transfusion，Minhang Hospital, Fudan University, Shanghai, 201199 China

[c] Center for Laboratory Medicine, Allergy center, Department of Transfusion medicine, Zhejiang Provincial People's Hospital (Affiliated People's Hospital), Hangzhou Medical College, Hangzhou, Zhejiang 310014, China

[d] Key Laboratory of Biomarkers and In Vitro Diagnosis Translation of Zhejiang Province, Hangzhou, Zhejiang 310063, China

[e] School of Medical Technology and Information Engineering, Zhejiang Chinese Medical University, Hangzhou, Zhejiang, 310053, China

[1]These authors contributed equally to this work.

[*]Correspondence: Zhen Wang, Youmin Ying, Kaiqiang Li

Email: wangzhen@hmc.edu.cn; ymying@zjut.edu.cn; likaiqiang@hmc.edu.cn

Abstract

Background

The imbalance in the gut-brain is strongly associated with psychiatric conditions related to inflammatory bowel disease (IBD), and an effective treatment approach has not been established. Current oral treatments are limited due to the spatial and functional divide between gut inflammation and central nervous system (CNS) issues.

Purpose

The purpose of this research was to investigate the therapeutic impact of extracellular vesicles derived from *Lindera aggregate* leaf (LALEVs) and root (LAREVs) in alleviating DSS-induced intestinal damage and behavioral disorders in mice.

Methods

Dextran sulfate sodium (DSS) was used to establish an acute ulcerative colitis (UC) mouse model, and the mice were administered LALEVs and LAREVs orally. After the oral intervention, comprehensive assessments were performed utilizing pathological, biochemical, and molecular biological approaches, alongside 16S rRNA sequencing and behavioral evaluations, to examine intestinal barrier integrity, gut microbiome composition, lipopolysaccharide (LPS) levels, and pro-inflammatory cytokine production. Behavioral assessments were conducted to assess anxiety-, depressive-like behaviors, and cognitive impairment, while neuroinflammatory responses were evaluated by monitoring microglial and astrocytic activation, neuronal injury, and neuroinflammation. Potential targets were explored by serum proteomics, Gene Set

Enrichment Analysis (GSEA), and network pharmacology, and verified by western blot.

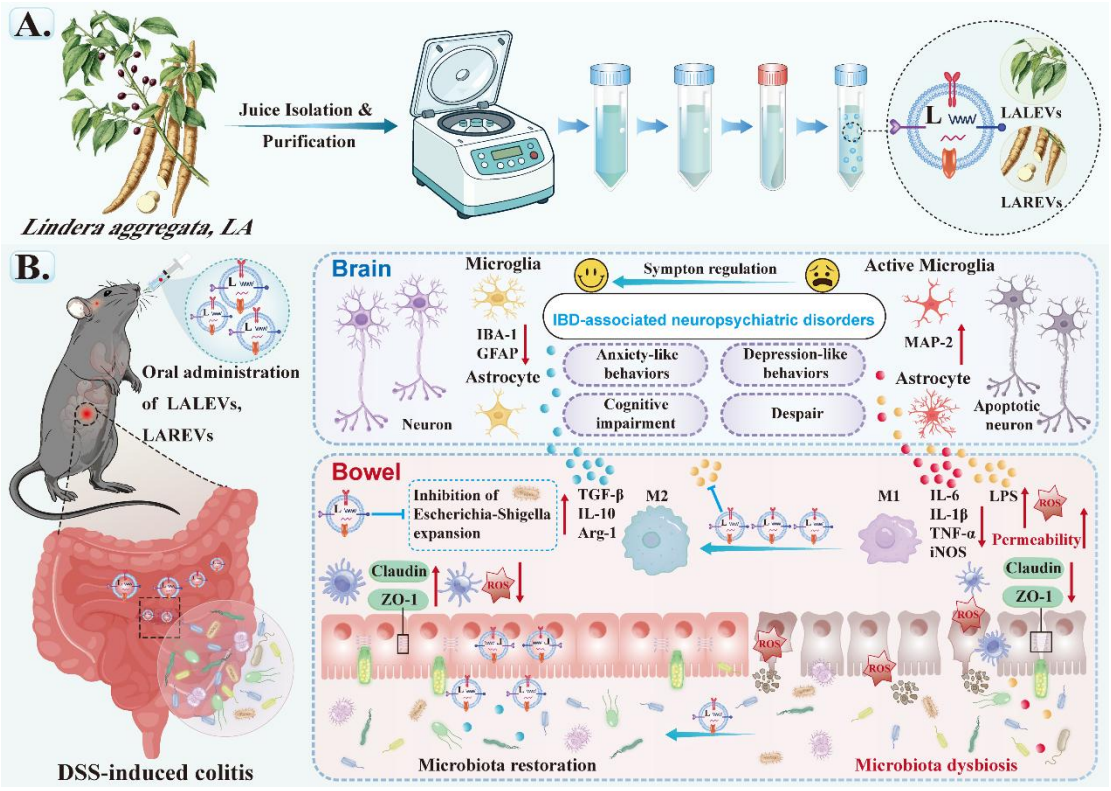
Results

Oral administration of LALEVs or LAREVs targeted inflamed colon, effectively restoring the compromised barrier. Colon length normalized, weight loss ceased, and inflammatory cytokines (TNF-α, IL-6, and IL-1β) were quieted. Behavioral tests indicated marked improvements in spontaneous activity and a substantial reduction in anxiety, depression-like behaviors, and cognitive impairment. Through by microbiota-gut-brain axis, LALEVs and LAREVs prevent LPS and inflammatory factors from entering the blood and suppress microglial and astrocyte activation in brain through modulating of TLR4/p38 MAPK axis, thereby reducing neuroinflammation and protecting against neural damage. Our work suggested that *Lindera aggregate*-derived extracellular vesicles could serve as a dual-target therapy for addressing IBD and psychiatric disorders.

Keywords

Inflammatory bowel disease, anxiety, depression and cognitive impairment, Plant-derived Extracellular Vesicles, microbiota-gut-brain axis

Graphical abstract.



Schematic illustration of the oral LALEVs or LAREVs with anti-inflammatory effects via microbiota-gut-brain axis for the treatment of IBD associated psychiatric disorders.

1 Introduction

Inflammatory bowel disease (IBD) is a chronic, immune-mediated disorder of the gastrointestinal tract[1, 2], comprising two principal forms: ulcerative colitis (UC) and Crohn's disease (CD). Beyond intestinal manifestations, accumulating evidence indicates a substantial burden of neuropsychiatric comorbidity, with anxiety and depressive disorders affecting as many as 35% of IBD patients[3]. In clinic, although about 30% of IBD patients are prescribed antidepressants off-label, there is insufficient clinical evidence to confirm their impact on IBD associated psychiatric symptoms[4]. The effectiveness in addressing IBD associated psychiatric disorders remain controversial and generally unsatisfactory.

The pathobiology of IBD is closely linked to gut microbiome dysbiosis, characterized by decreased microbial diversity and altered microbial composition[5, 6]. Clinical research reveals that IBD patients exhibit significant *Escherichia-Shigella* overgrowth, which secretes toxins and triggers pro-inflammatory signals. Concurrently, reduced levels of *Lactobacillus* and *Bifidobacterium* may compromise the intestinal barrier, allowing endotoxins like LPS to enter systemic circulation and potentially impair distal organ function[7, 8]. Recent studies indicate that increased levels of LPS and LBP, due to intestinal leakage, activate microglia and damage neurons in the brain, contributing to anxiety, depressive symptoms, and altered neural activity in IBD patients[9, 10]. Moreover, research has indicated that the regulation of microbiota-gut-brain axis (MGBA) axis could harmonize the crosstalk between the gut and brain[11-13]. Therefore, the modulation of the intestinal microbiota in MGBA seems to be a very

promising approach for treating IBD with psychiatric disorders.

Plant-derived extracellular vesicles (PDEVs) have shown potential as a therapeutic approach for IBD[14]. PDEVs derived from edible sources such as ginger, garlic, turmeric and Honeysuckle exert their anti-IBD effects by modulating the intestinal microenvironment homeostasis, including immune responses[15, 16], the intestinal barrier[17], and the gut microbiota[18, 19]. Beyond the well-recognized effects in IBD, PDEVs are now gaining attention for their potential applications in brain diseases and neuroinflammation. For instance, Panax notoginseng-derived PDEVs was very first study exploring PDEVs' effect on brain disease. It could enter the brain without modification [20]. Maca-derived PDEVs altered gut microbiota and metabolism via GTP-Cdc42/ERK and BDNF/TrkB/AKT pathways, improving depressive behaviors[21]. Honeysuckle-derived PDEVs show promise for oral delivery, attenuating both pathological symptoms and psychiatric disturbances in colitis mice[22]. Collectively, these observations underscore the therapeutic potential of medicinal PDEVs for psychiatric disorders associated with IBD.

Lindera aggregate (LA), a traditional Chinese herb whose roots and leaves have been used as traditional Chinese medicine or functional food, has a long history in treating IBD. Research indicates that LA significantly improves intestinal function and mitigates depressive-like behaviors [23]. Norisoboldine, a key bioactive component of LA, exhibits antidepressant-like properties in behavioral assessments[24] and alleviates both gastrointestinal and neuropsychiatric manifestations in slow transit constipation (STC) complicated by depression, an effect attributed to re-establishing intestinal

immune homeostasis and attenuating neuroinflammation[25]. Linderane, another major compound, has been demonstrated to reduce pain and anxiety caused by CFA, suppress inflammatory cytokine release, and inhibit microglial activation[26]. Despite these encouraging findings for LA in IBD and psychiatric disorders, research on LA-derived extracellular vesicles (LAEVs) remain scarce.

In this study, to explore the therapeutic potential of LAEVs, we isolated vesicles from the plant's leaf (LALEVs) and root (LAREVs), with a particular focus on the MGBA. We propose a therapeutic strategy centered on “gut-brain dual-region synergistic therapy” to alleviate IBD associated psychiatric disorders. We first validated that gut microbial dysbiosis constitutes a prominent pathological feature of IBD and is causally linked to central neuroinflammation via aberrant microglial activation. Subsequently, we comprehensively characterize our biomaterial and investigate the protective effects of LALEVs and LAREVs in IBD with psychiatric disorders. Our results demonstrated that oral administration of LALEVs or LAREVs targeted inflamed colon tissue, shifted macrophages from M1 to M2 phenotype, maintaining the integrity of the intestinal epithelium. LALEVs and LAREVs alleviated oxidative stress and inflammation, which helped correct gut microbiota imbalances caused by DSS, preserved the intestinal barrier, and lowered systemic LPS and pro-inflammatory cytokines due to barrier dysfunction. These effects further suppressed microglial and astrocytic activation, preserved neuronal integrity, and mitigated neuroinflammation via modulation of the MGBA, ultimately improving DSS-induced depressive-like behaviors and cognitive impairment.

2 Materials and methods

2.1 Reagents and materials

Fresh *Lindera aggregate* (commonly known as "Wuyao") were obtained from a local herbal market in Tiantai County (Taizhou, China). Lipopolysaccharide (LPS) was obtained from Sigma-Aldrich (Dorset, UK). Beyotime Biotechnology (Shanghai, China) supplied the fluorescent dyes Dil and DiR, Hoechst 33342, the Actin Tracker Green-488 probe, areactive oxygen species (ROS) assay kit, live/dead cell staining and nitric oxide (NO) detection kit. CCK-8 assay kit, Coomassie Brilliant Blue rapid staining kit, reverse transcription reagents were sourced from Nanjing Vazyme Biotech Company Co., Ltd. (Nanjing, China). Trizol reagent and the BCA protein assay kit were acquired from Thermo Fisher Scientific. ELISA kits for mouse IL-6 and TNF-α were procured from Shanghai Enzyme-linked Biotechnology Co., Ltd. (Shanghai, China). An antibody against iNOS was acquired from Abcam (Cambridge, UK). Antibodies against p38 and p-P38 were sourced from Cell Signaling Technology. The TLR4 antibody was obtained from Abmart (Shanghai, China). DSS was purchased from Bide Pharmatech Ltd. (Shanghai, China).

2.2 Cell lines

RAW264.7 mouse leukemia cells were obtained from Wuhan Pricella Life Science & Technology Co., Ltd., while HT-29 human colon cells were sourced from the Chinese Academy of Sciences Cell Bank. Both cell types were grown in high-glucose DMEM with 10% FBS, prepped and equilibrated to room temperature before use.

2.3 Animals

Healthy SPF-grade male C57BL/6 mice (20-22g, 6-8 weeks) were purchased from GemPharmatech Co., Ltd. (Jiangsu, China). The Animal Ethics Committee of Zhejiang Provincial People's Hospital (Approval No. 20240202200516621695) reviewed and approved all animal experimental procedures. The operators conducting the animal experiments held the Training Certificate for Laboratory Animal Technicians of Zhejiang Province (certificate No.x2403248).

2.4 Preparation and characterization of LAEVs

Fresh *Lindera aggregate* leaves were rinsed with deionized water and homogenized in pre-cold PBS. The homogenate was filtered and centrifuged. For *Lindera aggregate* root samples, fresh root tissues were first ground into a fine powder to minimize large particulates. The powder was suspended in PBS and stored at 4°C for 12 h, then filtered and centrifuged. The filtrates from both leaf and root preparations were separately subjected to differential centrifugation steps: 1,000 ×g for 30 min, 5,000 ×g for 30 min, and 15,000 ×g for 60 min to remove large contaminants including cells, protoplasts, plant fibers, cell debris, and large vesicles. The supernatant from the final centrifugation underwent additional centrifugation at 120,000 ×g for 1.5 h. The resulting pellet was then purified via a sucrose density gradient and centrifuged at 150,000 ×g for 2 h. The fraction between the 30% and 45% sucrose layers was collected, diluted with Tris-HCl buffer, and centrifuged at 5,000 ×g for 30 min to eliminate sucrose. The pellet was resuspended in PBS, sterilized using a 0.22 μm filter, and either utilized immediately or stored at -80°C.

Morphology of the purified LALEVs and LAREVs was observed by TEM

(HT7700, Hitachi, Japan). The zeta potential was assessed using DLS with a Zetasizer Nano ZSE (Malvern Instrument, UK). Particle size distribution and concentration measurement by Nanocoulter I instruments (Shenzhen, China).

The stability of LALEVs and LAREVs was evaluated by incubating them in simulated gastric and intestinal fluids at 37°C for 6 h. Particle size and zeta potential changes were then measured to assess vesicle aggregation or degradation across varying pH conditions.

2.5 *In vitro* cytotoxicity

Cytotoxicity was measured using a CCK-8 assay. RAW264.7 and HT-29 cells were exposed to LALEVs or LAREVs at protein concentrations between 0 and 400 μg/mL for 24 h, after which 10 μL CCK-8 reagent was added for 1 h. A microplate reader (BioTek, USA) was used to measure the absorbance at 450 nm.

Viability was additionally examined by live/dead staining. Cells cultured overnight in 6-well plates were treated with LALEVs or LAREVs for 24 h, rinsed with PBS, and incubated with Calcein-AM/PI solution following the manufacturer's protocol. Fluorescence signals were captured under a fluorescence microscope.

2.6 Cellular uptake

Dil dye was incubated with both LALEVs and LAREVs at 4°C for 1 h. Ultracentrifugation was used to remove free dye, after which the pellet was resuspended in PBS to produce Dil-labeled LALEVs and LAREVs. RAW264.7 cells (3×10^4 per well) were plated on poly-L-lysine-coated coverslips and maintained in 24-well plates. Cells were exposed to 200 μg/mL of either Dil-LALEVs or Dil-LAREVs for 8, 12, and

24 h. After the application, cells underwent washing, fixation, permeabilization, and staining with Actin Tracker Green and Hoechst dye. Coverslips were cleaned with PBS, mounted on slides using anti-fade medium, sealed, and allowed to air-dry. Cells were then imaged using a super-resolution microscope (Leica, Germany).

2.7 LPS-induced inflammatory model

An in vitro inflammatory model was established based on previously published protocols[27] and preliminary experiments. RAW264.7 cells were stimulated with LPS (1 μg/mL) while receiving LALEVs or LAREVs (200 μg/mL) for 24 h. A co-culture system was used to set up the macrophage-intestinal epithelial cell model: RAW264.7 cells were placed in the lower chamber and HT-29 cells in the upper chamber. Following 24 h LPS exposure with LALEVs or LAREVs, medium was refreshed, and macrophages were co-cultured with HT-29 cells for an additional 24 h.

2.8 RT-qPCR

RAW264.7 cells were cultured in 6-well plates (5×10^5/well) and treated for 24 h with LALEVs, LAREVs, LPS, or control medium. Harvested cells underwent Trizol-based RNA extraction, reverse transcription, and RT-qPCR on a 7500 Real-Time PCR System, $2^{-\Delta\Delta Ct}$ for quantification. Colon and hippocampal tissues were processed identically. Target primers are listed in Table S1.

2.9 ELISA assay

Macrophage culture supernatants from each co-culture group were collected. Corresponding mouse ELISA kits were used to measure inflammatory cytokine levels Concentrations were determined from a standard curve with absorbance at 450 nm. For

serum samples, the preparation and analytical procedures were identical to those applied to cell culture supernatants.

2.10 *In Vivo* Biosafety

C57BL/6 male mice acclimated and divided into three groups (Control, LALEVs, LAREVs). Body weights were recorded daily for 7 days throughout the experiment. LALEVs and LAREVs groups received 50 mg/kg of respective vesicles via oral gavage, while the control group received PBS. On day 8, blood samples were collected for serum analysis, and all mice were euthanized for organ collection and histopathological assessment.

2.11 Animal model and treatment

C57BL/6 male mice were randomized into four groups: (Control, DSS, LALEVs LAREVs). Except for Controls, all animals received 3% DSS in their drinking water for 7 days to induce acute colitis. The LALEVs and LAREVs groups were given 50 mg/kg of their respective treatments daily, while the Control and DSS groups received PBS. Clinical signs of colitis were monitored daily, and all mice were euthanized on day 8 for tissue collection.

2.12 Histopathological evaluation of colon tissues

Colon tissues were fixed with 4% PFA for H&E staining. For IHC, sections were performed using standard antigen retrieval and blocking, followed by overnight incubation with primary antibodies against ZO-1 and claudin at 4°C and subsequent HRP-conjugated secondary antibody/DAB-hematoxylin detection. Stained slides were then dehydrated, cleared, mounted with neutral balsam, and viewed under a

241 light microscope.

242 **2.13 Behavioral tests**

243 Behavioral experiments were conducted following the completion of LALEVs and
244 LAREVs treatments. Mice acclimated to the testing room for 30 min before testing.
245 Their behavioral performance was recorded and analyzed using the Tracking Master
246 software.

247 **Open field test（OFT）**

248 Each mouse was placed in a 50 × 50 × 40 cm arena for 8 min to explore freely,
249 with their movements tracked by an overhead camera. The arena was cleaned with
250 75% ethanol between sessions. Exploratory behavior and locomotion were evaluated
251 by measuring the total distance traveled and time spent in the center[28].

252 **Elevated plus-maze (EPM)**

253 The maze, shaped like a cross, had two open and two closed arms (each 30 × 5 cm),
254 with 15 cm high walls on the closed arms. Elevated 40 cm above the ground, mice
255 explored it for 10 min starting from the center towards an open arm. Anxiety was
256 assessed by tracking entries and time spent in the open and closed arms[29].

257 **Light-dark box (LDB)**

258 The apparatus comprised a light and a dark compartment connected by a small
259 door. Each mouse was positioned at the middle of e lit area and allowed to explore for
260 8 min. Anxiety and depression-like behaviors were evaluated by tracking time spent in
261 each compartment and the number of transitions[30].

262 **Novel object recognition test (NOR)**

The testing apparatus was the same as that used for the open field test. Initially, mice explored an empty arena for 10 minutes, after which they were exposed to two identical objects positioned 10 cm from the walls for another 10 minutes. Following a 1-hour interval, a novel object replaced one of the existing objects, and mice were given 5 min to explore. Exploration was characterized by the nose being directed within 2 cm of the object. Discrimination index was calculated using dedicated software.

Y-maze test (YMT)

The Y-maze featured three arms, each measuring 40 cm by 10 cm, arranged at 120° angles. Each mouse was positioned at the end of an arm facing the center and permitted to explore for 8 min. Arm entry sequences were documented, and the spontaneous alternation rate was computed to assess working memory.

2.14 Nissl staining

Brain tissues were processed by fixation in 4% paraformaldehyde, paraffin embedding, dewaxing, rehydration, and Nissl staining. After rinsing, sections were dehydrated, cleared, and mounted for microscopy. The morphology of the hippocampal dentate gyrus (DG) and cornu ammonis 1 (CA1) region was analyzed, and lesioned cells were quantified using ImageJ.

2.15 Immunofluorescence staining

RAW264.7 cells on poly-L-lysine-coated coverslips were treated as in Section 2.7, then fixed, permeabilized, blocked, and probed with primary antibodies at 4°C overnight followed by fluorophore-conjugated secondary antibodies. After DAPI mounting, cells were imaged by super-resolution confocal microscopy

For hippocampal immunofluorescence, sections were exposed to primary antibodies at 4 °C overnight, including MAP-2, GFAP, and Iba-1. Apply 4 °C overnight, followed by incubation with the second antibody. DAPI dye the nucleus. After mounting with DAPI-containing medium, sections were visualized by super-resolution confocal microscopy.

2.16 16S rRNA sequencing analysis

Gut microbiota in mouse cecal contents was profiled by 16S rRNA gene sequencing. Following DNA isolation, purity and concentration were assessed, and agarose gel electrophoresis was used for quality verification. The V3–V4 hypervariable region was PCR-amplified with universal primers. Amplicons were quantified and pooled into libraries, followed by high-throughput sequencing. Bioinformatic analyses were conducted on the Lianchuan Bio-Information Technology Co., Ltd. cloud platform (Hangzhou, China).

2.17 Serum proteomics analysis

Serum samples were collected and preprocessed using a high-abundance protein depletion kit to remove interfering proteins such as albumin. Total protein was extracted and quantified using the BCA method. An 80 μg protein aliquot was adjusted to 80 μL with ammonium bicarbonate, mixed with DTT, and heated. After cooling, IAA was added, and the sample was incubated. Trypsin was introduced for overnight digestion, and the reaction was stopped with formic acid. Peptides were desalted, dried, reconstituted, and analyzed by LC-MS/MS.

2.18 Western blotting

Following the sacrifice of the mice, brain tissues were collected and homogenized in RIPA buffer for protein extraction. Proteins were separated via SDS-PAGE, transferred to PVDF membranes, blocked with 5% skim milk, and treated with primary antibodies overnight at 4°C. The secondary antibody employed was anti-rabbit IgG, and signals were detected using chemiluminescence on a Bio-Rad imaging system.

2.19 Network pharmacology

Untargeted LC-MS/MS metabolomics was utilized to delineate the chemical profiles of LALEVs and LAREVs. Subsequent to metabolite database matching, compounds with predicted high gastrointestinal absorption and at least two drug-likeness criteria were identified as potential orally bioavailable ingredients through screening with the SwissADME database (https://www.swissadme.ch/) [31]. The putative targets of these compounds were inferred using the SwissTargetPrediction database (http://www.swisstargetprediction.ch/) applying a probability threshold of greater than 0.1. Disease-associated targets were extracted from the GeneCards database (https://www.genecards.org) using the search terms “UC”, “IBD”, “behavioral disorder”, “anxiety”, “depression”, and “Cognitive dysfunction”. After eliminating duplicates, overlapping targets between the compound-predicted and disease-related targets were identified as potential therapeutic targets for LALEVs and LAREVs. A protein-protein interaction network was subsequently constructed using the STRING database (https://string-db.org) to investigate the interactions among these targets. Finally, KEGG pathway enrichment analysis was performed to elucidate the signaling

pathways modulated by LAEVs and their underlying therapeutic mechanisms.

2.20 Statistical analysis

Statistical analyses were performed using GraphPad Prism 9.5, and results are expressed as mean ± SD. Significance between two experimental groups was assessed using Student's t-test, while one-way ANOVA was employed for analyses involving multiple groups. One-way ANOVA Significance levels are indicated as follows: $*P < 0.05$, $**P < 0.01$, and $***P < 0.001$.

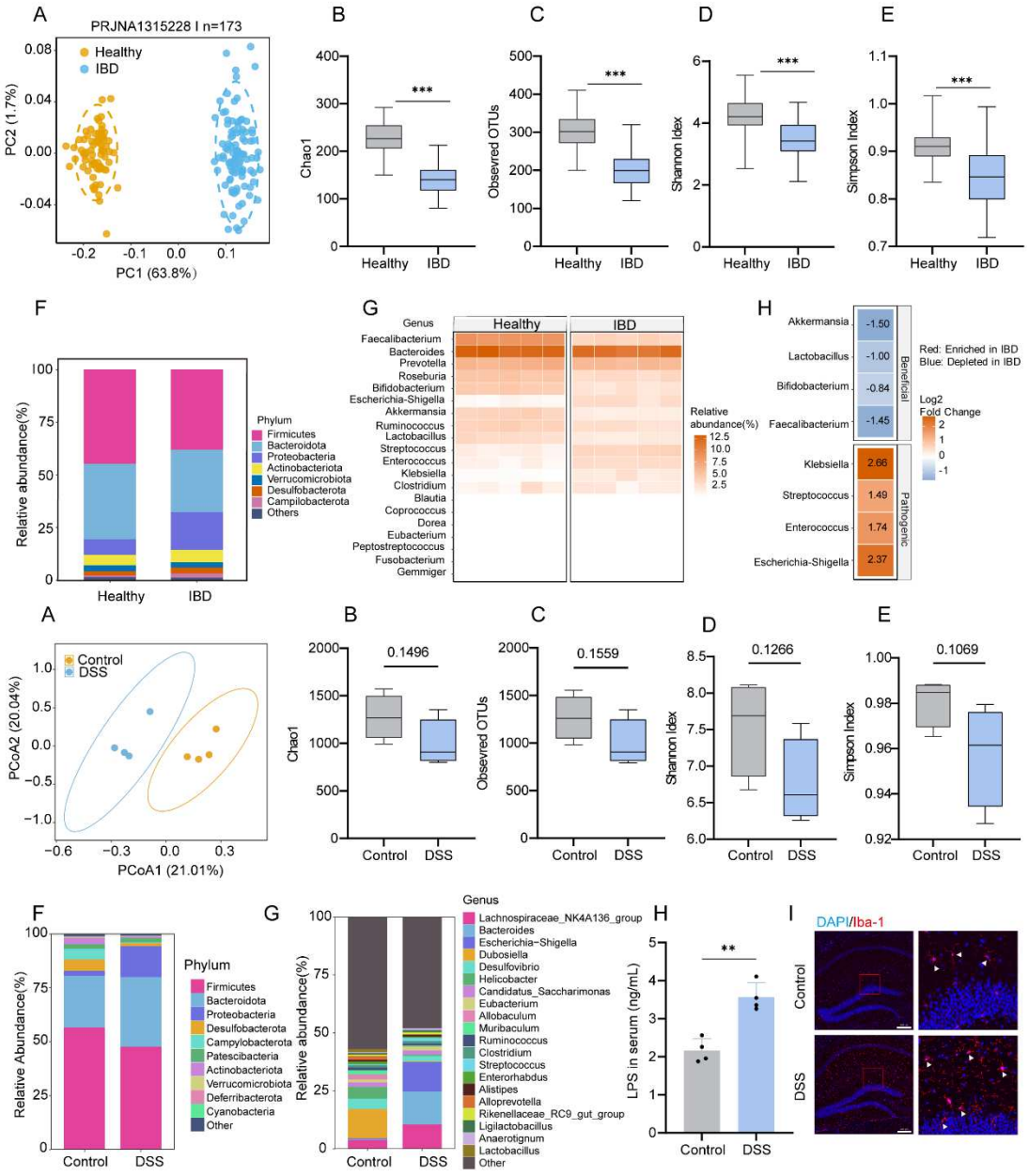
3 Results and Discussion

3.1 Characterization of gut microbiota alterations and their impact on the gut-brain axis in IBD

To characterize the gut microbiota alterations associated IBD, we first analyzed the metabolomic data derived from a 16S rRNA sequencing dataset (PRJNA1315228), which comprised 101 IBD patients and 72 healthy controls. PCoA demonstrated a clear distinction in the gut microbial composition between IBD patients and healthy controls (Fig. 1A). Compared with the healthy group, IBD patients exhibited a reduction in microbial richness and diversity (Fig. 1B-E), along with pronounced shifts in microbial community structure (Fig. 1F-G). These observations were further validated in two independent public datasets from murine colitis models (PRJNA1164042 and HRA004834, n = 23). Cross-cohort comparative analyses consistently revealed a similar pattern of gut microbiota alterations in colitis mice, characterized by a decreased abundance of potentially protective genera such as *Faecalibacterium*, *Akkermansia*, and *Bifidobacterium*, alongside an increased presence of the opportunistic pathogen

Escherichia-Shigella. Collectively, these results suggest that gut microbial dysbiosis is a prominent feature of IBD (Fig. S1).

It is now widely recognized that the gut microbiota and its metabolites (mainly neurotransmitters and precursors) implicate in the pathogenesis of neuroinflammation and various psychiatric disorders[32, 33]. To investigate the potential impact of gut microbial dysbiosis on IBD associated psychiatric disorder, we established an acute colitis mouse model using 3% DSS. 16S rRNA sequencing revealed that the microbiota alterations observed in our experimental colitis mice closely paralleled those identified in the public databases, typically in *Proteobacteria* and *Escherichia-Shigella* (Fig. 1I-O). Notably, the DSS group demonstrated a significant increase in serum LPS (Fig. 1P). And luminal bacterial products, such as LPS and tyrosine, were found to enter the systemic circulation, thereby inducing a state of low-grade systemic inflammation[34]. Additionally, we observed microglial activation in the hippocampus, with more Iba-1 positive cells and shorter processes (Fig. 1Q), indicating central neuroinflammation. These findings suggest that gut microbial dysbiosis-induced systemic inflammation can abnormally activate microglia in the brains of IBD patients.



367

368 Figure 1 Characterization of gut microbiota alterations and their impact on the gut-brain axis in IBD.

369 (A-H) 16S rRNA sequencing dataset (PRJNA1315228) (A) PCoA analysis. Chao1 (B), Observed

370 OTUs (C), Shannon (D) and Simpson (E) indices of gut microbiome. Histogram of gut microbiota

371 relative abundance at the phylum level (F) and heatmap at the genus level(G). (H) Heatmap of log2

372 fold changes of differential genera. (I-O) 16S rRNA sequencing in DSS-induced mice (n=4). (I)

373 PcoA analysis. Chao1 (J), Observed OTUs (K), Shannon (L) and Simpson (M) indices of gut

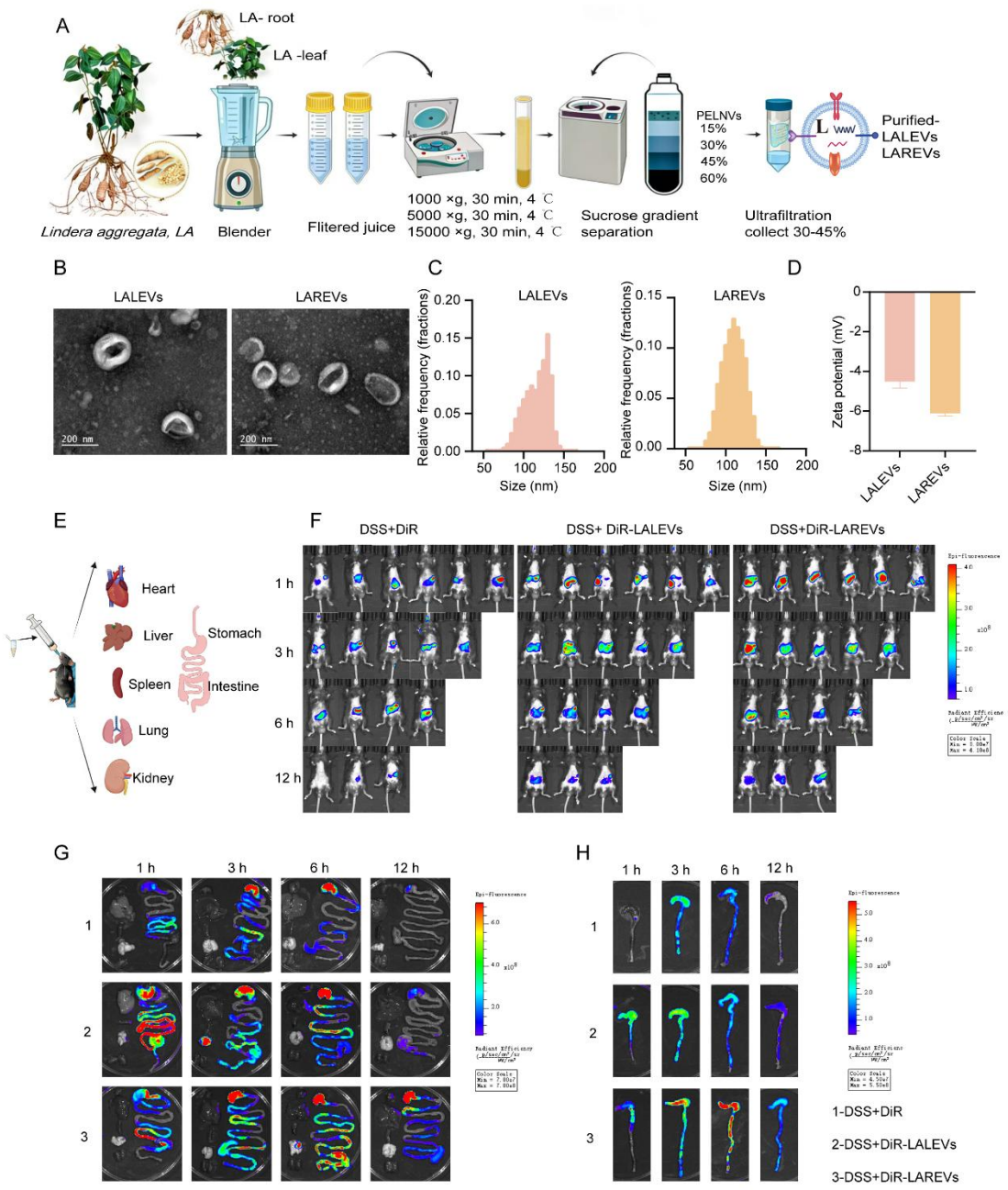
microbiome. Histogram of gut microbiota relative abundance at the phylum level (N) and genus level(O). (P) ELISA detection of serum LPS levels. (Q)Immunofluorescence images of DAPI (blue) and Iba-1 (red) in hippocampus, $^{**}P < 0.01$, and $^{***}P < 0.001$.

3.2 Physicochemical properties and colon-targeting ability of LAEVs

Based on the above findings, we next sought to explore the intervention of LAEVs targeting MGBA axis imbalance in the treatment of colitis and associated psychiatric disorders. As shown in Fig. 2A, LALEVs and LAREVs were isolated through sequential differential centrifugation followed by sucrose density gradient purification. TEM revealed that both types of LAEVs exhibited typical spherical or cup-shaped morphology with a bilayer membrane structure and relatively uniform size (Fig. 2B). Coulter nano-particle size analysis showed that the average particle sizes of LALEVs and LAREVs were 125 nm and 110 nm, respectively (Fig. 2C), falling within the typical range of dietary exosome-like nanoparticles. Zeta potential is an important characteristic for evaluating nanoparticle stability. Generally, nanoparticles with Zeta potential values between -30 mV and +30 mV are considered stable[35]. Both types of LAEVs carried a negative surface charge, with Zeta potentials of -4.92 ± 0.78 mV for LALEVs and -6.03 ± 0.07 mV for LAREVs, indicating that the isolated LALEVs and LAREVs were stable (Fig. 2D). The challenging physiological environment of the gastrointestinal tract frequently results in drug degradation, the harsh physiological environment of the gastrointestinal tract often leads to drug degradation, limiting oral bioavailability. Both LALEVs and LAREVs exhibited only minor changes in zeta potential and particle size in simulated gastric and intestinal fluids, with size variations

remaining within 10% (Fig. S2). These results indicate that both LALEVs and LAREVs concluded an excellent stability and could maintain their integrity during gastrointestinal absorption.

Targeted accumulation of orally administered nanomedicines in the inflamed colon is essential for therapeutic efficacy in IBD. To assess in vivo biodistribution, LALEVs and LAREVs were labeled with the DiR dye for in vivo tracing, and their fluorescence intensity was monitored using imaging systems at 1, 3, 6, 12h (Fig. 2E). Compared with free DiR, both LALEVs and LAREVs exhibited markedly enhanced intestinal accumulation and retention in colitis mice (Fig. 2F). Ex vivo imaging further revealed stronger fluorescence signals in the intestine and minimal distribution in other major organs, indicating predominant gastrointestinal retention (Fig. 2G). Time-course imaging of the colon confirmed specific and sustained accumulation of LALEVs and LAREVs, but not in bare DiR (Fig. 2H). These results suggest that LALEVs and LAREVs exhibited a stronger colon targeting and retention ability.



410

411 Figure 2 Physicochemical properties and colon-targeting ability of LAEVs. (A) Schematic

412 illustration depicting the stepwise preparation protocol of LALEVs and LAREVs. (B) Morphology

413 observed by TEM, scale bar = 200 nm. (C) Particle size distribution measured by Nanocoulter I

414 instrument. (D) Zeta potential analyzed by DLS. (E) Schematic diagram of in vivo biodistribution.

415 (F) In vivo fluorescence imaging of mice in each group at different time points, ex vivo fluorescence

416 imaging of major organs (heart, liver, spleen, lung, kidney, and gastrointestinal tract) (G) and the

colon (H).

3.3 *In vitro* modulation of the inflammatory microenvironment by LAEVs

Macrophages are crucial regulators in the inflammatory microenvironment of IBD [36], this study examines the impact of LALEVs and LAREVs on the polarization of RAW264.7 macrophages. First, we tested the effective cellular uptake levels. As shown in Fig. S3, both Dil-LALEVs and Dil-LAREVs were efficiently internalized by macrophages and predominantly localized in the cytoplasm. Subsequently, the i*n vitro* cytocompatibility efficacy of LALEVs and LAREVs were evaluated. Both LALEVs and LAREVs exhibited negligible cytotoxicity toward RAW264.7 and HT-29 cells, even at concentrations as high as 200 μg/mL (Figure S4). As expected, we found that LALEVs and LAREVs exerted anti-inflammatory effects.

In LPS-stimulated macrophages, treatment with LALEV or LAREVs led to a marked reduction in the mRNA expression of IL-1β, IL-6, and TNF-α, while concurrently resulting in a increase in the levels of TGF-β and IL-10 (Fig. 3A, B). And immunofluorescence results demonstrated that LALEVs or LAREVs significantly reduced iNOS expression and increased Arg-1 expression (Fig. 3C, D), indicating that LAEVs had effects on macrophage polarization.

To simulate the inflammatory microenvironment of intestinal epithelial cells under IBD conditions, a macrophage-intestinal epithelial cell co-culture system was established (Fig. 3E). ELISA analysis demonstrated that both LALEVs and LAREVs decreased IL-6 and TNF-α levels produced by macrophages (Fig. 3F). In the presence of LALEVs or LAREVs, the macrophage-derived secretory products reduced the NO

concentration in the HT-29 cell supernatant and ROS levels (Fig. 3G-I) indirectly alleviating the inflammatory response of intestinal epithelial cells. Intestinal epithelial integrity relies on cell migration. A wound-healing assay showed that over time, wound width decreased in all groups. At 24 h, the Control group had the widest wound, while LAREVs treatment resulted in the narrowest wound and the strongest pro-migratory effect (Fig. 3J, K), indicating that LAEVs promote intestinal epithelial repair through modulation of the inflammatory microenvironment.

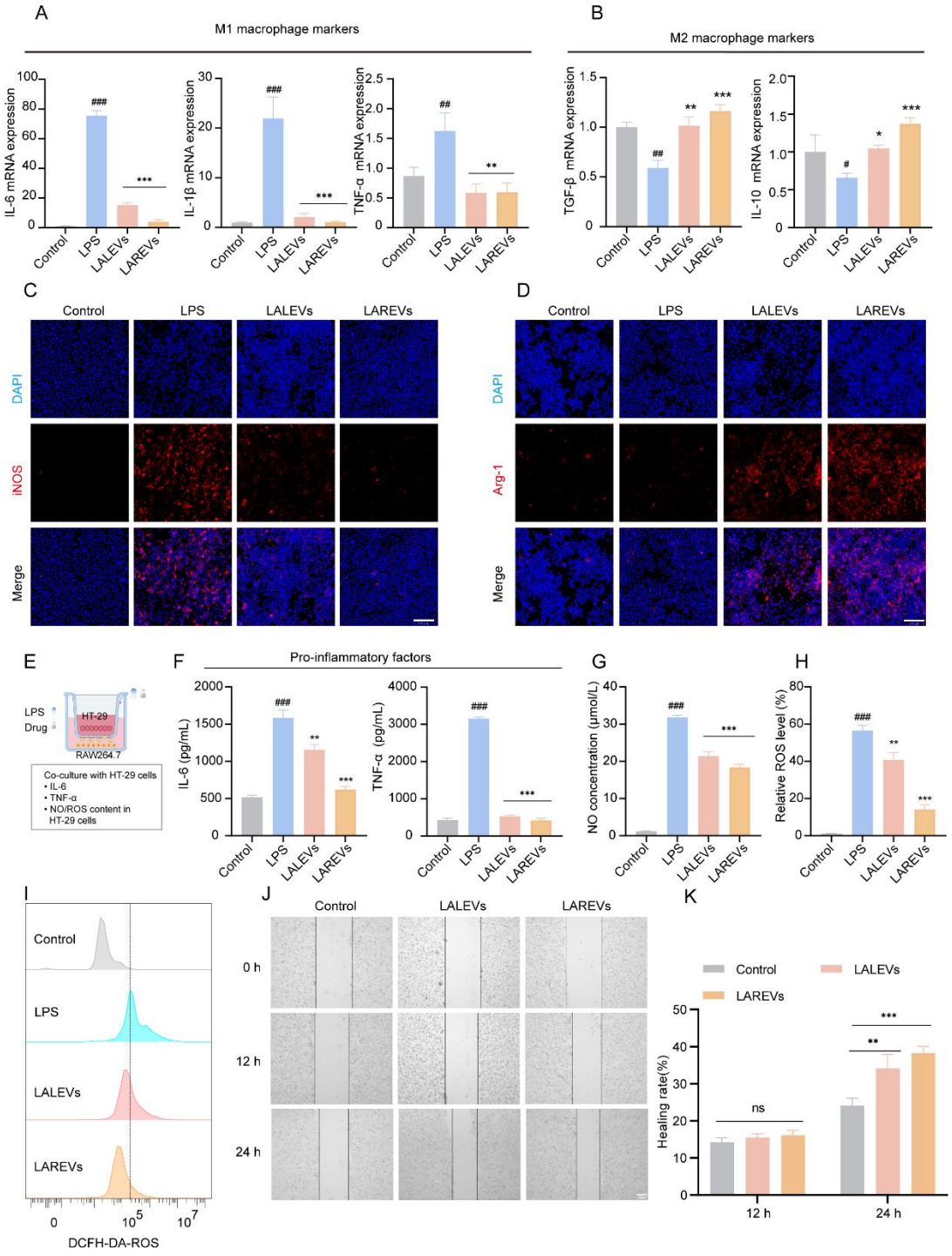


Figure 3 In vitro anti-inflammatory abilities of LALEVs or LAREVs. RT-qPCR analysis of the relative expression levels of M1 and M2 macrophage markers mRNAs in LPS-induced RAW264.7 cells from indicated groups (A, B). Representative images of immunofluorescence staining of iNOS (C) andArg-1 in RAW264.7, scale bar 100 μm. (E) Schematic diagram of the co-culture system of macrophages and intestinal epithelial cells. (F) IL-6 and TNF-α concentrations in macrophage

supernatants. (G) NO levels in the supernatant of HT-29 cells. (H, I) Flow cytometry peak plots and quantification of ROS content. (J, K) Scratch wound healing assays of HT-29cells treated with various conditions. #$P < 0.05$，##$P < 0.01$，###$P < 0.001$ vs. Control group; *$P < 0.05$, **$P < 0.01$, ***$P < 0.001$ vs LPS group, n=3. The concentration of LPS was 1 μg/mL. LALEVs and LAREVs were 200μg/mL.

3.4 LAEVs alleviate DSS induced colitis

Based on the dose-dependent efficacy of PDEVs against colitis (10~50 mg/kg) as previously reported[37-39]. In this study, we orally administered LALEVs and LAREVs at 50 mg/kg in a mouse model of colitis (Figure 4A). Relative to the DSS group, o LALEVs or LAREVs treatment resulted in a significant mitigation of the reduction in hematochezia (Fig. 4B) and colon shortening (Fig. 4C, D). Concurrently, LAEVs could also substantially inhibit body weight loss (Fig. S5A), decrease disease activity index (DAI) scores (Fig. S5D), restore normal food and water intake (Fig. S5C, D) and alleviate spleen enlargement (Fig. S5E, F). Moreover, histopathological analysis of colon tissues revealed that DSS induced elicited extensive epithelial injury and crypt architectural distortion, whereas mice receiving LALEVs or LAREVs preserved an intact epithelial barrier structure (Fig 4E, F). Restoration of the intestinal barrier function was further evidenced by the upregulated expression of tight junction components ZO-1 and claudin after LAEV intervention (Fig. 4G), similar to the results in mRNA levels (Fig. 4H, I). RT-qPCR analysis of colon tissues further showed that DSS markedly elevated the transcript levels of TNF-α, IL-6, and IL-1β, which were effectively brought down by LALEV or LAREV treatment (Fig. 4J-L). Collectively,

these results imply that LALEVs and LAREVs exert beneficial effects on intestinal barrier preservation and colitis alleviation.

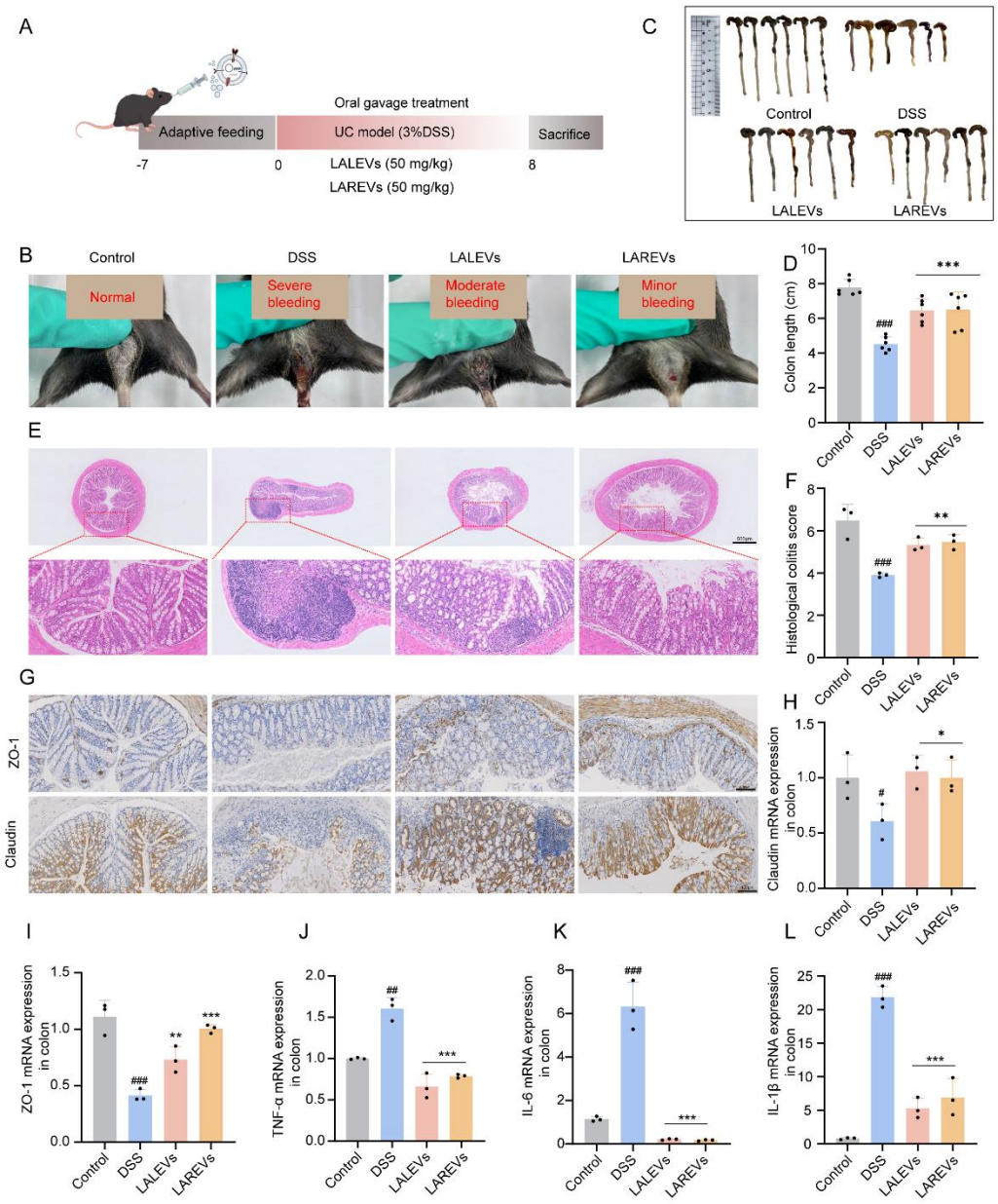


Figure 4 Anti-inflammatory effects of LAEVs against intestinal inflammation. (A)Schematic illustration of DSS-induced chronic colitis mouse model. (B) Images of rectal bleeding of mice in different groups during treatment. Images of the colon tissues (C) and colon length (D) of mice in different groups. (E) H&E staining, Scale bar = 500 μm, n=3. (F) histological scores. (G) Immunohistochemical staining of tight junction proteins, Scale bars=100 μm, n=3. (H, I) mRNA

expression of tight junction proteins ZO-1 and Claudin in colon tissues detected by RT-qPCR. (J-L) The levels of inflammatory cytokines in colon tissues, n=3. #P < 0.05，##P < 0.01，###P < 0.001 vs. Control group; *P < 0.05, **P < 0.01, ***P < 0.001 vs. DSS group, n=6.

3.5 Behavior changes in the colitis mouse model

Emerging evidence indicates that intestinal barrier disruption could transmit inflammatory signals to the CNS, potentially leading to depression and anxiety-like behaviors in IBD[40-42]. We further We conducted an evaluation of anxiety, depressive-like behaviors, and cognitive-related behaviors in relation to colitis-associated psychiatric disorders (Fig. 5A).

In OFT, DSS mice demonstrated restricted peripheral movement, fewer center entries, and a marked reduction in total distance traveled. In contrast, LALEVs or LAREVs treatments increased locomotor activity, center exploration, and total distance traveled (Fig. 5C). Consistently, in EPM, DSS mice exhibited pronounced avoidance of the open arms, whereas LALEVs or LAREVs increased both open-arm time and entries (Fig. 5B). In LDB test, DSS reduced light-zone occupancy and intercompartment transitions, effects that were significantly reversed by LALEV or LAREV treatment (Fig. 5D). These findings indicate that LALEVs or LAREVs treatments effectively reduce colitis-related behavioral despair and anxiety.

The YMT and NOR tests were used to evaluate cognitive function. In the YMT, DSS treatment significantly decreased the spontaneous alternation rate, whereas oral administration of LALEVs or LAREVs restored this parameter, indicating improved spatial working memory (Fig. 5E). In the NOR test, DSS mice exhibited reduced

exploration of the novel object and a lower recognition index, suggesting impaired cognitive performance. In contrast, both LALEVs and LAREVs increased the recognition index and restored preference for the novel object to levels comparable with those of control mice (Fig. 5F). Collectively, these findings demonstrate that LALEVs and LAREVs alleviate DSS-induced cognitive impairment in colitis mice.

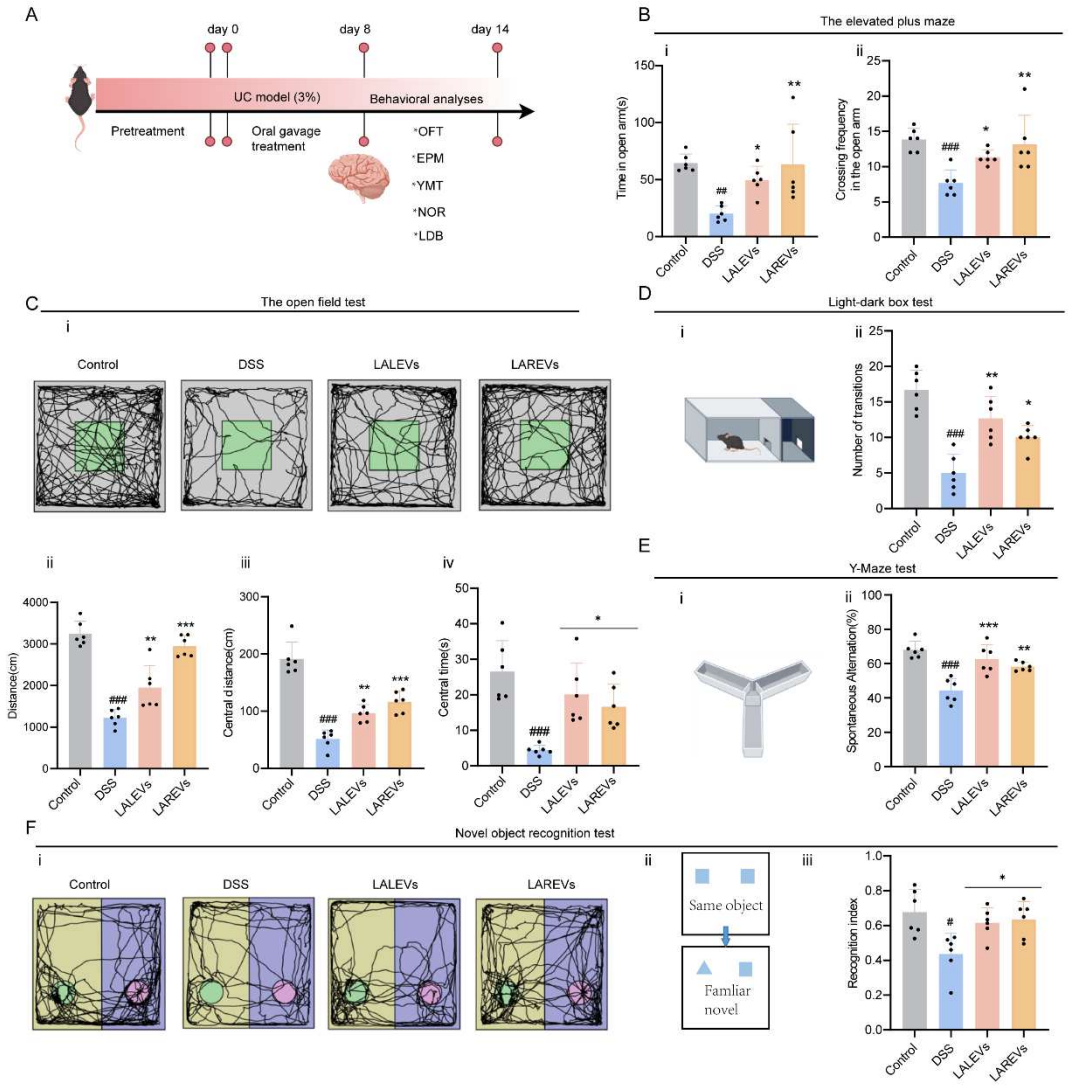


Figure 5. LAEVs prevents DSS-induced anxiety, depressive behavioral changes and recognition impairment. (A) Schematic illustration of model building and intervention. (B) Time spent in the open arms (i) and frequency of entries (ii) into the open arms in EPM. (C) Example of movement traces(i), total distance traveled (ii), distance traveled in the central area (iii) and time spent in the

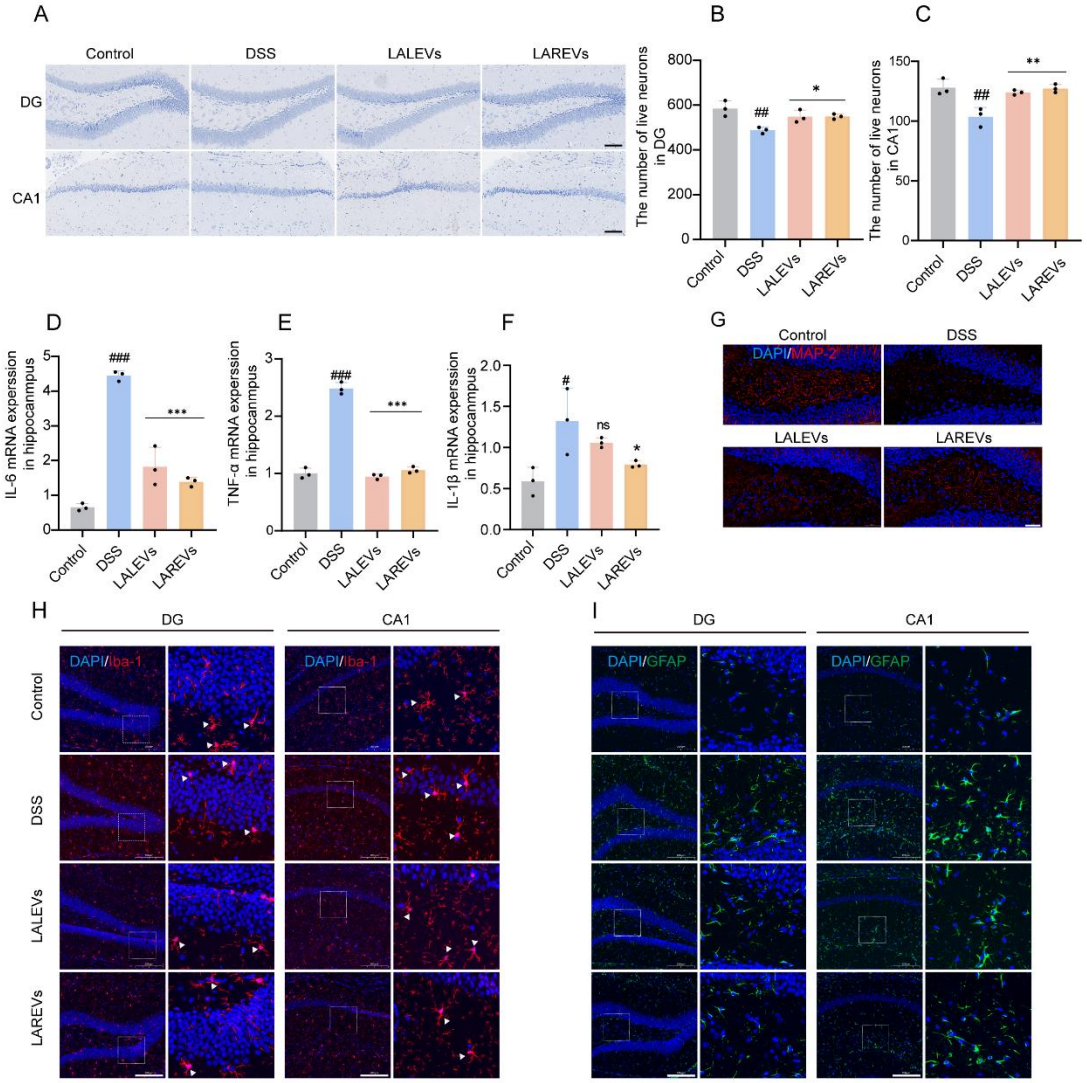
central area (iv) in each group in the open field test. (D) Schematic diagram of the LDB (i) and frequency of transitions to the light compartment (ii). (E) Schematic diagram of the YMT (i) and spontaneous alternation rate of mice in each group in YMT (ii). (F) Example of movement traces (i), Schematic diagram of the NOR (ii) and recognition index of mice in each group in NOR (iii). #$P < 0.05$，##$P < 0.01$，###$P < 0.001$ vs. Control group; *$P < 0.05$, **$P < 0.01$, ***$P < 0.001$ vs. DSS group, n=6.

3.6 LAEVs mitigates hippocampal damage and neuroinflammation

The hippocampus, a central hub for emotional regulation and cognitive processing, is particularly vulnerable to neuronal injury, especially within the DG and CA1 subfields, and this susceptibility is closely tied to the onset of depressive and related psychiatric disorders[43, 44]. Nissl staining showed LAEVs reduced viable neurons in DG and CA1 regions in DSS mice (Fig. 6A-C), indicating neuronal degeneration. Neuro-inflammation worsens mature neurons by disrupting neurotransmitter balance, leading to anxiety-like behaviors[45, 46]. Consistently, MAP-2 immunostaining, which labels mature hippocampal neurons, showed a pronounced reduction in fluorescence intensity in DSS mice, and this reduction was effectively reversed by LALEVs or LAREVs (Figure 6G). Furthermore, LALEVs or LAREVs also reduced hippocampal inflammation levels, including IL-1β, IL-6, and TNF-α, in DSS-treated mice (Fig. 6D-F). These results indicate that LAEVs may against inflammatory-induced neuron damage in the hippocampus.

Previous research has established hat colitis can trigger the activation of hippocampal astrocytes and microglia, thereby fostering a neuroinflammatory

536 microenvironment[47]. Immunofluorescence staining of the hippocampus was
537 conducted utilizing Iba-1 to identify microglia and GFAP to identify astrocytes. In the
538 DSS group, microglia exhibited an amoeboid activated morphology, characterized by
539 shortened processes and reduced branching complexity. In contrast, LALEVs or
540 LAREVs group displayed more resting microglia, as evidenced by elongated processes
541 and the restoration of a ramified network architecture, indicating a dampened cerebral
542 immune response (Fig. 6H). The DSS group displayed a significant downregulation of
543 GFAP fluorescence intensity along with astrocyte activation, indicating that DSS
544 induced severe neuroinflammation. After treatment of LALEVs or LAREVs, the GFAP
545 labeling intensity was significantly reduced (Fig. 6I). These findings indicate that mice
546 subjected to DSS exhibit behaviors indicative of anxiety, depression-like symptoms,
547 and cognitive impairment, which are correlated with neuronal damage in the
548 hippocampus and cerebral inflammation. Conversely, supplementation with LALEVs
549 or LAREVs appears to promote neuronal repair and mitigate neuroinflammation in the
550 brain.



551

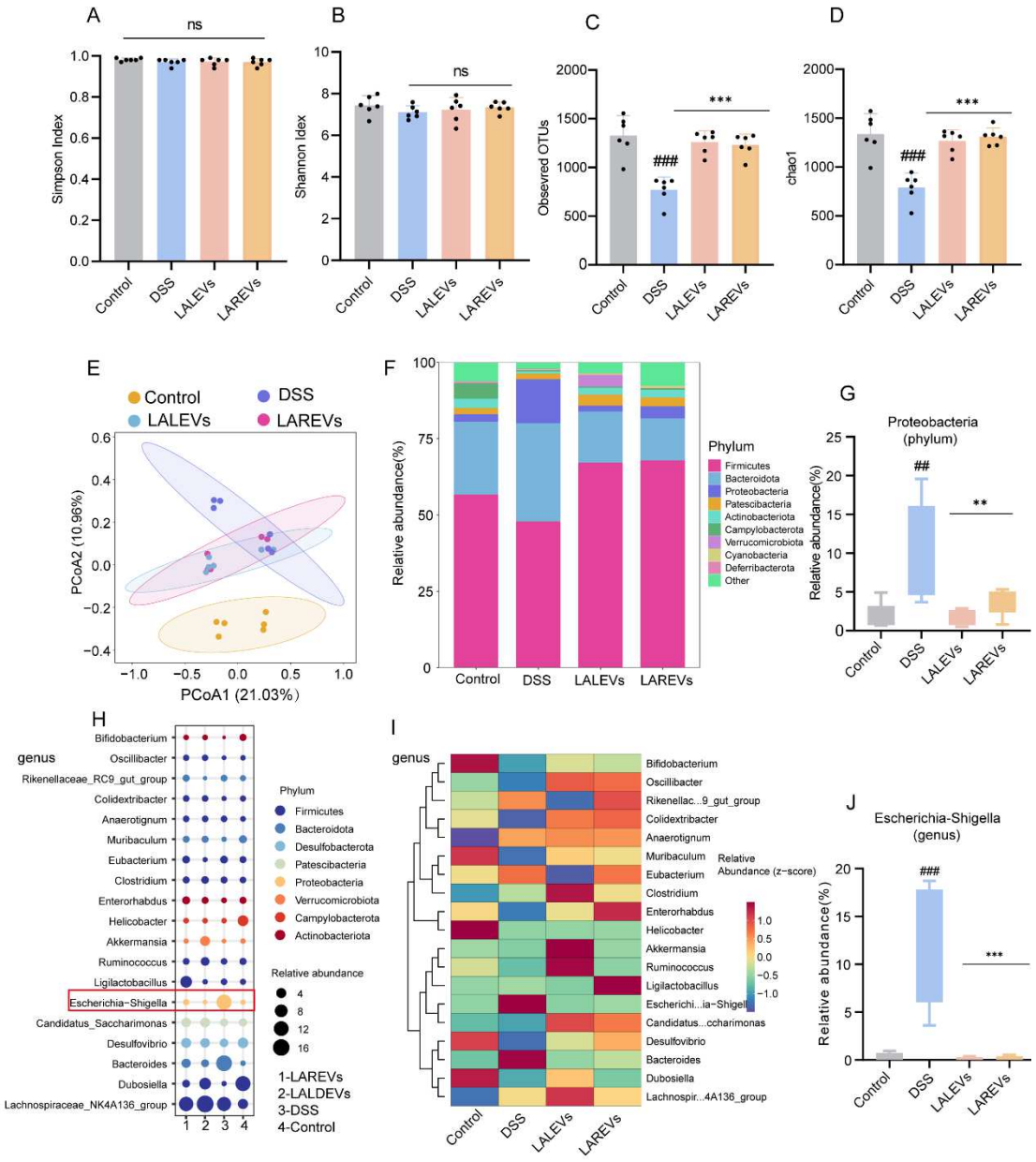
552 Figure 6 Alleviation effects of LAEVs on hippocampal damage and neuroinflammation in DSS-
553 induced mice. (A-C) Representative images of Nissl staining and quantification of hippocampal
554 neurons with lesions, scale bar = 100 μm. (D-F) mRNA expression levels of IL-1β, IL-6, and TNF-
555 α in hippocampal tissues detected by RT-qPCR. Immunofluorescence staining results of mature
556 neurons (MAP-2, red, scale bar = 50 μm) (G), microglia (Iba-1, red, scale bar = 200 μm) (H) and
557 astrocyte (GFAP, green, scale bar = 200 μm) (I) in the hippocampi of mice in different groups. #P
558 < 0.05, ###P < 0.001 vs. Control group; *P < 0.05, **P < 0.001 vs. DSS group, n = 3.

559 **3.7 Modulation of gut microbiota**

Section 3.1 was demonstrated that DSS-induced colitis replicates the dysbiosis associated with IBD, characterized by an expansion of *Proteobacteria* and *Escherichia-Shigella*, a reduction in beneficial microbial taxa, and increased serum LPS levels. Given that this dysbiosis may contribute to dysfunction in the MGBA, we subsequently evaluated the potential of LALEVs or LAREVs to mitigate these microbial alterations by 16S rRNA.

Microbial alpha diversity was profiled to assess community complexity, encompassing both richness and evenness. As shown in Fig. 7A and 7B, the Shannon and Simpson indices did not differ significantly among the groups, reflecting comparable species evenness. However, the DSS group exhibited reduced Observed OTUs and Chao1 index, indicating decreased species richness due to DSS-induced colitis. LALEVs and LAREVs treatments significantly improved these indices (Fig. 7C, D). PCoA analysis demonstrated a clear distinction between DSS group samples and the Control group, highlighting significant gut microbiota changes due to DSS. LALEVs and LAREVs treatments resulted in a shift of the samples towards the Control group, indicating a successful reversal of DSS-induced dysbiosis and restoration of microbial balance (Fig. 7E). At the phylum level, the DSS group exhibited an increased abundance of *Bacteroidetes* and *Proteobacteria*. (Fig. 7F, G), Enrichment of *Proteobacteria* has been established as a hallmark of gut dysbiosis and epithelial barrier compromise[48, 49], whereas overgrowth of *Bacteroidetes* has also been closely associated with intestinal inflammation[50]. LALEVs or LAREVs intervention suppressed these aberrant enrichments and increased *Firmicutes* abundance. At the

family level (Fig. 7H-J), DSS group showed marked *Escherichia-Shigella* enrichment, consistent with IBD reports. This pathogen triggers systemic inflammation via TLR4/MyD88/NF-κB and correlates with Alzheimer's and BBB impairment[51]. As part of the Enterobacteriaceae family, it can invade intestinal cells and weaken the gut barrier[52]. More importantly, as a Gram-negative bacterium, its cell wall component LPS serves as a potent immunostimulatory molecule. and DSS-induced gut barrier damage permits LPS entry into the bloodstream, causing systemic inflammation and central dysfunction. LALEVs or LAREVs treatment decreased *Escherichia-Shigella* levels. Conversely, DSS reduced beneficial genera (*Bifidobacterium*, *Dubosiella*, *Akkermansia*). *Bifidobacterium* produces GABA/5-HT precursors and modulates tryptophan metabolism for anxiolytic effects. *Dubosiella* declines in colitis; *Akkermansia* sustains barrier integrity and exerts anti-inflammatory actions, with its recovery directly linked to anxiety relief[53]. Following intervention with LALEVs or LAREVs, the abundances of the aforementioned beneficial bacterial abundance were restored to varying degrees. Collectively, LAEVs appear to enhance microbial diversity while suppressing *Escherichia-Shigella*, thereby alleviating intestinal inflammation and improving brain function.



599

600 Figure 7 Gut microbiome amelioration in mice with DSS-induced UC after LAEVs treatment. (A)

601 Simpson index. (B) Shannon index. (C) Microbial richness, observed OTUs. (D) Chao1 index. (E)

602 PCoA analysis showing β-diversity of the gut microbiome. Each point represents one mouse.

603 Stacked bar plots (F) and relative abundance statistics of Proteobacteria (G) at the phylum level.The

604 bubble plot (H), cluster heatmap(I) and relative abundance statistics of *Escherichia-Shigella* (J)at

605 the genus level, #$P < 0.05$， ##$P < 0.01$， ###$P < 0.001$ vs. Control group; **$P < 0.01$, ***$P < 0.001$

606 vs. DSS group, n=6.

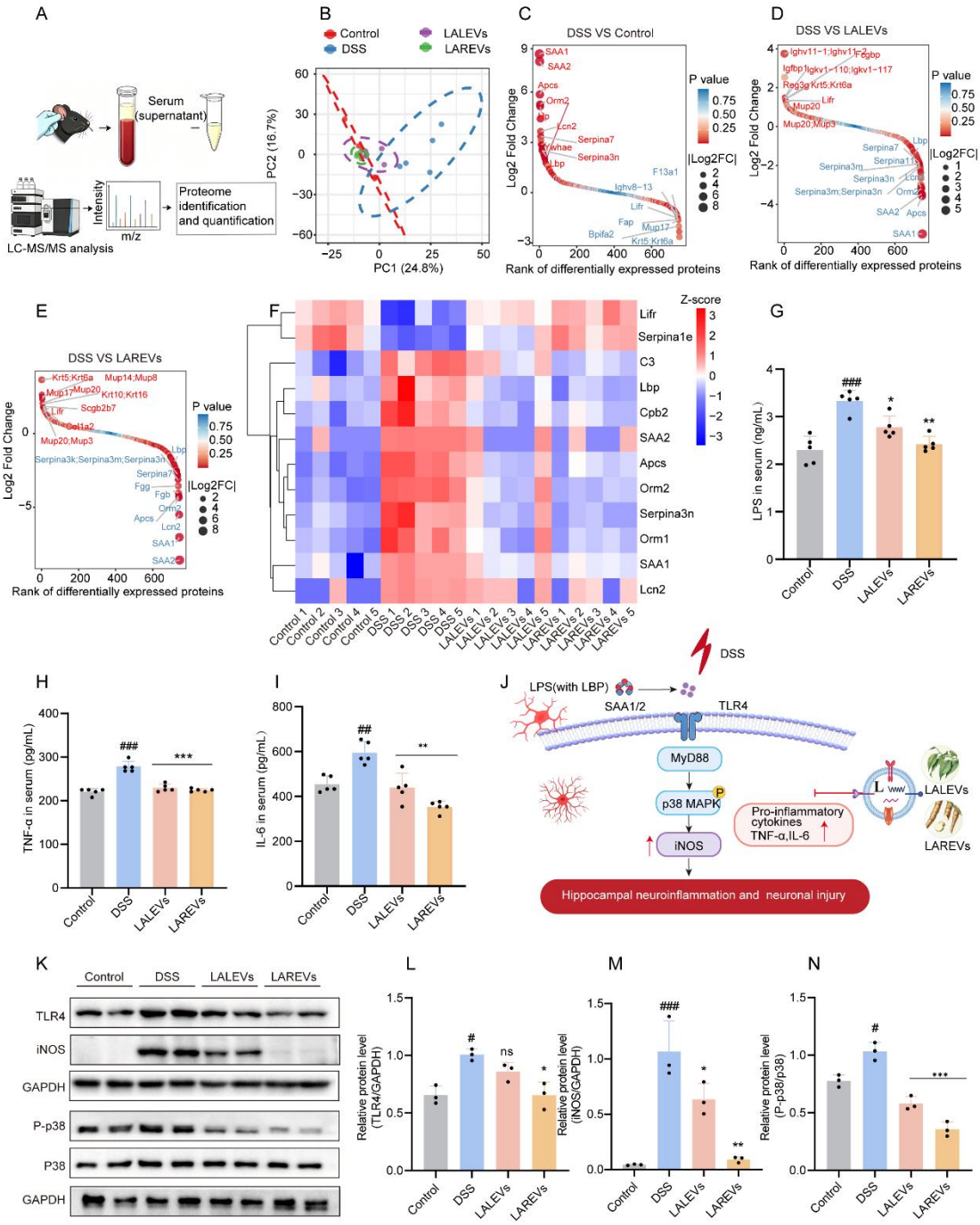
3.8 LAEVs attenuate DSS-induced colitis and associated psychiatric disorders via inhibition of the TLR4/p38 MAPK signaling pathway

To further dissect the mechanistic underpinnings, serum proteomic profiling was performed (Fig.8A). PCA resolved the DSS, LALEVs, and LAREVs groups into distinct clusters (Figure 8B). Differential abundance analysis subsequently uncovered a panel of proteins with significant alterations (Fig.8C-F). Nobly, in comparison to the Control group, the expression of serum amyloid A1/2 (SAA1/2) and amyloid P component (APCS), hallmark proteins of colitis, was upregulated more than sixfold in DSS-treated mice (Fig.8C), whereas LALEVs or LAREVs treatment led to a significant downregulation of these two hallmark proteins by more than fourfold (Fig.8D, E). SAA1/2, as endogenous ligands for Toll-like receptor 4 (TLR4)[54], can cross the intact BBB[55, 56] and promote barrier leakage[57], subsequently activating microglia and astrocytes to produce pro-inflammatory cytokines within the brain [58].

Concurrently, the simultaneous elevation of serum LBP (a key molecule responsible for LPS recognition) (Fig S6A), alongside elevated LPS levels in DSS mice, supports the translocation of LPS from the intestinal lumen into the systemic circulation (Fig.8F, G), indicating an increased load of bacteria-derived antigens[59]. The elevated serum TNF-α and IL-6 further substantiate the systemic inflammation (Fig.8H, I). LPS identified as a TLR-4 ligand, binds to TLR4 with the assistance of LBP, leading to detrimental effects on brain function[60]. In addition, the marked reduction of Lifr in DSS mice was consistent with the observed neuroinflammation and hippocampal neuronal damage (Fig S6B). LALEVs or LAREVs treatment restored Lifr expression

(Fig. 8F), which may help re-establish neuroprotective signaling and support neuronal survival.

GSEA further enriched the Toll-like receptor signaling pathway (Fig. S7), prompting TLR4 as the key receptor. This hypothesis was explored using metabolomic profiling and network pharmacology approaches. Results indicated LALEVs and LAREVs were rich in terpenoids, flavonoids, and alkaloids. Leveraging these findings, we identified 2317 and 2305 potential bioactive targets for LALEVs and LAREVs, respectively, and found 246 and 258 overlapping DEGs. KEGG mapped these DEGs to MAPK and TLR pathways (Fig S8). Western blot in brain tissue (Fig. 8K-N) confirmed DSS upregulated TLR4, p38 MAPK, and iNOS versus Controls, indicating central TLR4-p38 axis activation, whereas LALEV or LAREV treatment reversed this effect. In short, the above results all demonstrated LAEVs suppress the transmission of intestinal inflammation to the CNS by inhibiting the TLR4/p38 MAPK signaling pathway.



643

644 Figure 8 Serum proteomic profiling. (A) Schematic diagram of serum proteomic profiling. (B)

645 Principal component analysis (PCA) plot. (C-E) Volcano plot revealing differentially expressed

646 proteins. (F) Heatmap of key target protein expression. ELISA measurement of LPS (G), TNF-α (H)

647 and IL-6 (I) protein levels in serum from each group. (J) LALEVs or LAREVs suppress the

648 transmission of intestinal inflammation to the central nervous system by inhibiting the TLR4/p38

MAPK signaling pathway. (K-N) Western blot images and quantitative analysis, n=3. ##$P < 0.01$, ###$P < 0.001$ vs. Control group; **$P < 0.01$, **$P < 0.001$ vs. DSS group, n = 5.

3.9 Oral Biosafety of LAEVs

Excellent biocompatibility is essential for advancing orally administered nanoparticles into animal studies. Under normal physiological conditions, the organ-to-body weight ratio remains relatively constant; however, toxicological effects can lead to fluctuations in organ weights, thereby altering organ index. Body weights were comparable among the LALEVs, LAREVs, and Control groups (Fig. S9A), and no significant alterations in organ indices were observed, implying that neither LALEVs nor LAREVs caused toxic injury in mice (Fig. S9B). Furthermore, a hemolysis assay demonstrated that red blood cells remained intact with increasing concentrations, indicating excellent hemocompatibility (Fig. S9C, D). Meanwhile, oral administration of LALEVs or LAREVs did not cause significant changes in serum biochemical parameters indicative of liver function (ALT, AST, ALB, and TP) and kidney function (Ur and Cr) (Fig. S9E, F). Furthermore, histopathological analysis by H&E staining of major organs (heart, liver, spleen, lung, and kidney) in the LALEVs or LAREVs groups remained unaffected (Fig. S9G). These findings demonstrate the excellent biosafety profile of LAEVs, highlighting their substantial potential for development as a targeted therapeutic agent for UC.

4 Conclusion

In summary, our study highlights that LALEVs and LAREVs, isolated and purified from natural plant *Lindera aggregate* leaves and roots, represent a viable therapeutic

candidate for ameliorating colitis and associated psychiatric disorders, with a particular emphasis on the MGBA. These nanovesicles exhibit substantial potential for large-scale production, harbor a broad spectrum of bioactive phytochemicals, and exhibit a favorable safety profile. LALEVs and LAREVs can effectively reprogram macrophage phenotypes, promoting a transition from M1 to M2. They also lowered inflammatory mediator output, reduced oxidative injury, and improved the inflammatory microenvironment. In a DSS-induced acute colitis, oral LALEVs or LAREVs survived the harsh digestive environment and adhered persistently to inflamed colonic tissue. This local effect restored barrier function and markedly decreased pro-inflammatory cytokine and LPS release, interrupting inflammatory signaling from the colon to the brain. Concurrently, LALEVs and LAREVs mitigated DSS-induced hippocampal pathological injury and neuroinflammation, thereby preserving neuronal plasticity and suppressing the excessive activation of microglia and astrocytes. These protective effects culminated in the alleviation of anxiety, depressive-like behaviors, and cognitive impairments. Collectively, these beneficial outcomes are achieved through modulation of the MGBA and inhibition of the TLR4/p38 MAPK signaling driven neural injury, thereby conferring dual amelioration of both the intestinal symptoms of DSS-induced colitis and the accompanying psychiatric disorders.

Funding

This work was partially supported by National Natural Science Foundation of China (82502781), Medical and Health Science Program of Zhejiang Province (2024KY636, 2025HY0113), Zhejiang Province Natural Science Foundation

(LQ22H190004) and the Pioneer and Leading Goose R&D Project of Zhejiang Province (No. 2026C04014).

Author contributions

Xiaoting Zhang: Original draft, Methodology, Jigeng Cao: Original draft, Tingting Hu: Methodology, Chengwen He: Investigation, Wei Xu: Formal analysis, Ke Hao: Visualization, Aibo Xu: Data curation, Kaixuan Li: Supervision, Qian Tong: Supervision, Zhen Wang: Funding acquisition, Youmin Ying: review & editing, Kaiqiang Li: Project administration, Funding acquisition, Writing - review & editing.

Data availability

The datasets used in this study are available from the corresponding author upon reasonable request.

Conflicts of interest

The authors have no conflicts of interest to declare.

Declaration of generative AI and AI-assisted technologies in the manuscript preparation process

In preparing this manuscript, DeepSeek was employed by the first author solely as a language-editing aid to improve sentence expression and readability in selected parts of this manuscript. The author subsequently checked and revised the text where necessary and bears full responsibility for the final published version.

References

1 Molodecky NA, Soon IS, Rabi DM, Ghali WA, Ferris M, Chernoff G, et al. Increasing incidence and prevalence of the inflammatory bowel diseases with time, based on systematic review.

715 Gastroenterology. 2012;142(1):46-54.e42; quiz e30.

716 2 Kaplan GG. The global burden of IBD: from 2015 to 2025. Nat Rev Gastroenterol Hepatol.

717 2015;12(12):720-7.

718 3 Barberio B, Zamani M, Black CJ, Savarino EV, Ford AC. Prevalence of symptoms of anxiety

719 and depression in patients with inflammatory bowel disease: a systematic review and meta-analysis.

720 Lancet Gastroenterol Hepatol. 2021;6(5):359-70.

721 4 Di Vincenzo F, D'Onofrio AM, Del Gaudio A, Chiera E, Ferrajoli GF, Pesaresi F, et al.

722 Psychopharmacological Therapy Positively Modulates Disease Activity in Inflammatory Bowel

723 Disease: A Systematic Review. Int J Mol Sci. 2025;26(13).

724 5 Petracco G, Faimann I, Reichmann F. Inflammatory bowel disease and neuropsychiatric

725 disorders: Mechanisms and emerging therapeutics targeting the microbiota-gut-brain axis.

726 Pharmacol Ther. 2025;269:108831.

727 6 Xiao Y, Chen X, Liao J, Wang J, Lu L, Chen H, et al. Dismantling the Necroptotic Engine: An

728 Oral Theranostic Nanosponge for Ulcerative Colitis. Adv Mater. 2026:e16297.

729 7 White Z, Cabrera I, Mei L, Clevenger M, Ochoa-Raya A, Kapustka I, et al. Gut inflammation

730 promotes microbiota-specific CD4 T cell-mediated neuroinflammation. Nature.

731 2025;643(8071):509-18.

732 8 Solanki R, Karande A, Ranganathan P. Emerging role of gut microbiota dysbiosis in

733 neuroinflammation and neurodegeneration. Front Neurol. 2023;14:1149618.

734 9 Lu J, Jin K, Chen B, Wang R, Hu F, Hu S, et al. A Synergistic Hydrogel-Microalgae Platform

735 for Dual-Targeting of Intestinal and Neuroimmune Dysfunction in Inflammatory Bowel Disease.

736 Adv Sci (Weinh). 2026:e23551.

737 10 Atanasova K, Knödler LL, Reindl W, Ebert MP, Thomann AK. Role of the gut microbiome in
738 psychological symptoms associated with inflammatory bowel diseases. Semin Immunopathol.
739 2025;47(1):12.
740 11 Yuan X, Chen B, Duan Z, Xia Z, Ding Y, Chen T, et al. Depression and anxiety in patients with
741 active ulcerative colitis: crosstalk of gut microbiota, metabolomics and proteomics. Gut Microbes.
742 2021;13(1):1987779.
743 12 Xu L, Li Y, He Y. The variation characteristics of fecal microbiota in remission UC patients
744 with anxiety and depression. Frontiers in Microbiology. 2023;Volume 14 - 2023.
745 13 Lee S-H, Han C, Shin C. IUPHAR review: Microbiota-gut-brain axis and its role in
746 neuropsychiatric disorders. Pharmacological Research. 2025;216:107749.
747 14 Li J, Luo T, Wang D, Zhao Y, Jin Y, Yang G, et al. Therapeutic application and potential
748 mechanism of plant-derived extracellular vesicles in inflammatory bowel disease. J Adv Res.
749 2025;68:63-74.
750 15 Kim J, Zhang S, Zhu Y, Wang R, Wang J. Amelioration of colitis progression by ginseng-
751 derived exosome-like nanoparticles through suppression of inflammatory cytokines. J Ginseng Res.
752 2023;47(5):627-37.
753 16 Yin L, Yan L, Yu Q, Wang J, Liu C, Wang L, et al. Characterization of the MicroRNA Profile
754 of Ginger Exosome-like Nanoparticles and Their Anti-Inflammatory Effects in Intestinal Caco-2
755 Cells. J Agric Food Chem. 2022;70(15):4725-34.
756 17 Gao C, Zhou Y, Chen Z, Li H, Xiao Y, Hao W, et al. Turmeric-derived nanovesicles as novel
757 nanobiologics for targeted therapy of ulcerative colitis. Theranostics. 2022;12(12):5596-614.
758 18 Zhu Z, Liao L, Gao M, Liu Q. Garlic-derived exosome-like nanovesicles alleviate dextran

759 sulphate sodium-induced mouse colitis via the TLR4/MyD88/NF-κB pathway and gut microbiota
760 modulation. Food Funct. 2023;14(16):7520-34.
761 19 Wang Y, Zhou Y, Wu Q, Li Y, Huang Y, Yu K, et al. Honeysuckle-Derived Nanovesicles
762 Regulate Gut Microbiota for the Treatment of Inflammatory Bowel Disease. Adv Sci (Weinh).
763 2025;12(45):e05208.
764 20 Li S, Zhang R, Wang A, Li Y, Zhang M, Kim J, et al. Panax notoginseng: derived exosome-
765 like nanoparticles attenuate ischemia reperfusion injury via altering microglia polarization. J
766 Nanobiotechnology. 2023;21(1):416.
767 21 Hong R, Luo L, Wang L, Hu ZL, Yin QR, Li M, et al. Lepidium meyenii Walp (Maca)-derived
768 extracellular vesicles ameliorate depression by promoting 5-HT synthesis via the modulation of gut-
769 brain axis. Imeta. 2023;2(3):e116.
770 22 Wu A, Chu Q, Ding L, Zeng Y, Shao L, Wang Y, et al. Honeysuckle-derived nanovesicles
771 alleviate inflammatory bowel disease-associated neuropsychiatric disorders via the gut-brain axis.
772 Theranostics. 2026;16(13):7419-41.
773 23 Wang X, Zhang X, Xie W, Wang Y, Zang S, Ban Z, et al. Lindera aggregata improves intestinal
774 function and alleviates depressive behaviors through the BDNF/TrkB/CREB signaling pathway
775 induced by CUMS in mice. Brain Research. 2025;1846:149295.
776 24 Li L, Kan W, Zhang Y, Wang T, Yang F, Ji T, et al. Quantitative proteomics combined
777 independent PRM analysis reveals the mitochondrial and synaptic mechanism underlying
778 norisoboldine's antidepressant effects. Transl Psychiatry. 2024;14(1):400.
779 25 Wu B, Wu J, Bai X, Zhou Q, Wang X. Mechanistic insights into the effects of Norisoboldine
780 on intestinal immunity and neuroinflammation in a mouse model of slow transit constipation with

781 depression. Journal of Ethnopharmacology. 2026;354:120479.

782 26 Chen Y, Qin Y, Gao Y, Wang S, Wang Q, Tang X, et al. Linderane Attenuates Complete
783 Freund's Adjuvant-Induced Pain and Anxiety in Mice by Restoring Anterior Cingulate Cortex
784 Microglia M2 Polarization through Activating Cannabinoid 2 Receptor. ACS Pharmacology &
785 Translational Science. 2024;7(3):797-808.

786 27 Linghu KG, Ma QS, Zhao GD, Xiong W, Lin L, Zhang QW, et al. Leocarpinolide B attenuates
787 LPS-induced inflammation on RAW264.7 macrophages by mediating NF-κB and Nrf2 pathways.
788 Eur J Pharmacol. 2020;868:172854.

789 28 Song AQ, Gao B, Fan JJ, Zhu YJ, Zhou J, Wang YL, et al. NLRP1 inflammasome contributes
790 to chronic stress-induced depressive-like behaviors in mice. J Neuroinflammation. 2020;17(1):178.

791 29 Zhou F, Jiang H, Kong N, Lin J, Zhang F, Mai T, et al. Electroacupuncture Attenuated Anxiety
792 and Depression-Like Behavior via Inhibition of Hippocampal Inflammatory Response and
793 Metabolic Disorders in TNBS-Induced IBD Rats. Oxid Med Cell Longev. 2022;2022:8295580.

794 30 Zhu Y, Wang F, Han J, Zhao Y, Yu M, Ma M, et al. Untargeted and targeted mass spectrometry
795 reveal the effects of theanine on the central and peripheral metabolomics of chronic unpredictable
796 mild stress-induced depression in juvenile rats. J Pharm Anal. 2023;13(1):73-87.

797 31 Luo X, Zhang X, Xu A, Yang Y, Xu W, Cai M, et al. Mechanistic Insights into the Anti-Glioma
798 Effects of Exosome-Like Nanoparticles Derived from Garcinia Mangostana L.: A Metabolomics,
799 Network Pharmacology, and Experimental Study. Int J Nanomedicine. 2025;20:5407-27.

800 32 Yano Jessica M, Yu K, Donaldson Gregory P, Shastri Gauri G, Ann P, Ma L, et al. Indigenous
801 Bacteria from the Gut Microbiota Regulate Host Serotonin Biosynthesis. Cell. 2015;161(2):264-76.

802 33 Joo MK, Lee JW, Woo JH, Kim HJ, Kim DH, Choi JH. Regulation of colonic neuropeptide Y

803 expression by the gut microbiome in patients with ulcerative colitis and its association with anxiety-
804 and depression-like behavior in mice. Gut Microbes. 2024;16(1):2319844.
805 34 Devereaux J, Robinson AM, Stavely R, Davidson M, Filippone RT, Ephraim R, et al.
806 Dysregulation of cellular metabolism within the gut-brain axis is associated with behavioural
807 changes in chronic intestinal inflammation. J Neuroinflammation. 2025;22(1):216.
808 35 Ou X, Wang H, Tie H, Liao J, Luo Y, Huang W, et al. Novel plant-derived exosome-like
809 nanovesicles from Catharanthus roseus: preparation, characterization, and immunostimulatory
810 effect via TNF-α/NF-κB/PU.1 axis. J Nanobiotechnology. 2023;21(1):160.
811 36 Zhang K, Guo J, Yan W, Xu L. Macrophage polarization in inflammatory bowel disease. Cell
812 Commun Signal. 2023;21(1):367.
813 37 Zhu MZ, Xu HM, Liang YJ, Xu J, Yue NN, Zhang Y, et al. Edible exosome-like nanoparticles
814 from portulaca oleracea L mitigate DSS-induced colitis via facilitating double-positive
815 CD4(+)CD8(+)T cells expansion. J Nanobiotechnology. 2023;21(1):309.
816 38 Li Y, Shao S, Zhou Y, Wang Y, Zheng W, Wang H, et al. Oral administration of Folium
817 Artemisiae Argyi-derived exosome-like nanovesicles can improve ulcerative colitis by regulating
818 intestinal microorganisms. Phytomedicine. 2025;137:156376.
819 39 Wu H, Pang M-m, Li Y-l, Huang J-j, Geng S-z, Hong J-h, et al. Flos sophorae immaturus
820 exosome-like nanovesicles alleviate ulcerative colitis by attenuating intestinal oxidative stress and
821 inflammation through activating Aryl hydrocarbon receptor via gut microbiota and tryptophan
822 metabolism regulation. Journal of Nanobiotechnology. 2026;24(1):132.
823 40 Collins SM, Surette M, Bercik P. The interplay between the intestinal microbiota and the brain.
824 Nature Reviews Microbiology. 2012;10(11):735-42.

825 41 He H, Qin Q, Xu F, Chen Y, Rao S, Wang C, et al. Oral polyphenol-armored nanomedicine for
826 targeted modulation of gut microbiota–brain interactions in colitis. Science Advances.
827 2023;9(21):eadf3887.
828 42 Miller AH, Haroon E, Felger JC. Therapeutic Implications of Brain–Immune Interactions:
829 Treatment in Translation. Neuropsychopharmacology. 2017;42(1):334-59.
830 43 Tartt AN, Mariani MB, Hen R, Mann JJ, Boldrini M. Dysregulation of adult hippocampal
831 neuroplasticity in major depression: pathogenesis and therapeutic implications. Mol Psychiatry.
832 2022;27(6):2689-99.
833 44 Lan J, Wang J, Huang S, Li C, Deng Z, Hao Z, et al. Neuropeptide SP protects against colitis
834 and linked anxiety-like behavior through the putative roles of gut microbiota and metabolite inositol.
835 Nat Commun. 2026;17(1):295.
836 45 Takahashi K, Nakagawasai O, Nemoto W, Odaira T, Sakuma W, Onogi H, et al. Effect of
837 Enterococcus faecalis 2001 on colitis and depressive-like behavior in dextran sulfate sodium-treated
838 mice: involvement of the brain-gut axis. J Neuroinflammation. 2019;16(1):201.
839 46 Chen Y, Shui M, Li H, Guo M, Yuan Q, Hao W, et al. Inflammation-targeted delivery of
840 probiotics for alleviation of colitis and associated cognitive disorders through improved vitality and
841 colonization. Biomaterials. 2025;318:123163.
842 47 Vitali R, Prioreschi C, Lorenzo Rebenaque L, Colantoni E, Giovannini D, Frusciante S, et al.
843 Gut-Brain Axis: Insights from Hippocampal Neurogenesis and Brain Tumor Development in a
844 Mouse Model of Experimental Colitis Induced by Dextran Sodium Sulfate. Int J Mol Sci.
845 2022;23(19).
846 48 Litvak Y, Byndloss MX, Tsolis RM, Bäumler AJ. Dysbiotic Proteobacteria expansion: a

847 microbial signature of epithelial dysfunction. Curr Opin Microbiol. 2017;39:1-6.

848 49 Shin NR, Whon TW, Bae JW. Proteobacteria: microbial signature of dysbiosis in gut

849 microbiota. Trends Biotechnol. 2015;33(9):496-503.

850 50 Fansler RT, Wu Y, Zhu W. Friend or foe? Contextualizing Bacteroides through the lens of niche

851 remodeling. Trends Microbiol. 2026;34(3):318-29.

852 51 Eslami M, Adampour Z, Fadaee Dowlat B, Yaghmayee S, Motallebi Tabaei F, Oksenych V, et

853 al. A Novel Frontier in Gut-Brain Axis Research: The Transplantation of Fecal Microbiota in

854 Neurodegenerative Disorders. Biomedicines. 2025;13(4).

855 52 Sansonetti PJ. Rupture, invasion and inflammatory destruction of the intestinal barrier by

856 Shigella, making sense of prokaryote–eukaryote cross-talks1. FEMS Microbiology Reviews.

857 2001;25(1):3-14.

858 53 Rosell-Cardona C, Cryan JF, Clarke G, Kittel-Schneider S. Host-microbiome relationship in

859 depression: can human induced pluripotent stem cells play a role in unravelling mechanisms? npj

860 Biofilms and Microbiomes. 2025;11(1):117.

861 54 Facci L, Chemello C, Marcolin E, Franceschini D, Scarin N, Pagetta A, et al. Serum amyloid

862 A1 directly engages TLR4/MD-2 to trigger neuroinflammatory signaling in microglia cultures.

863 International Immunopharmacology. 2026;180:116710.

864 55 Erickson MA, Jude J, Zhao H, Rhea EM, Salameh TS, Jester W, et al. Serum amyloid A: an

865 ozone-induced circulating factor with potentially important functions in the lung-brain axis. Faseb

866 j. 2017;31(9):3950-65.

867 56 Jang WY, Lee BR, Jeong J, Sung Y, Choi M, Song P, et al. Overexpression of serum amyloid

868 a 1 induces depressive-like behavior in mice. Brain Res. 2017;1654(Pt A):55-65.

869 57 Matsumoto J, Dohgu S, Takata F, Iwao T, Kimura I, Tomohiro M, et al. Serum amyloid A-
870 induced blood-brain barrier dysfunction associated with decreased claudin-5 expression in rat brain
871 endothelial cells and its inhibition by high-density lipoprotein in vitro. Neurosci Lett.
872 2020;738:135352.
873 58 Barbierato M, Borri M, Facci L, Zusso M, Skaper SD, Giusti P. Expression and Differential
874 Responsiveness of Central Nervous System Glial Cell Populations to the Acute Phase Protein Serum
875 Amyloid A. Scientific Reports. 2017;7(1):12158.
876 59 Gao C-Y, Pan Y-J, Su W-S, Wu C-Y, Chang T-Y, Yang F-Y. Abdominal ultrasound stimulation
877 alleviates DSS-induced colitis and behavioral disorders in mice by mediating the microbiota–gut–
878 brain axis balance. Neurotherapeutics. 2025;22(2):e00494.
879 60 Kalyan M, Tousif AH, Sonali S, Vichitra C, Sunanda T, Praveenraj SS, et al. Role of
880 Endogenous Lipopolysaccharides in Neurological Disorders. Cells. 2022;11(24).

Supplementary Files

This is a list of supplementary files associated with this preprint. Click to download.

- Supplementarymaterial.docx